RSC Advances

PAPER

View Article Online
View Journal | View Issue

Cite this: *RSC Adv.*, 2024, **14**, 15929

An ambipolar PEDOT-perfluorinated porphyrin electropolymer: application as an active material in energy storage systems†

Elizabeth Bermúdez Prieto,‡[a] Edwin J. González López, ‡[b] Claudia A. Solis, ‡[a] Jhair C. Leon Jaramillo,‡[a] Lorena P. Macor, [a] Rodrigo E. Domínguez,[c] Yohana B. Palacios,[b] Silvestre Bongiovanni Abel,[d] Edgardo N. Durantini, [b] Luis A. Otero,[a] Miguel A. Gervaldo*[a] and Daniel A. Heredia *[b]

The development of functional organic materials is crucial for the advancement of various fields, such as optoelectronics, energy storage, sensing, and biomedicine. In this context, we successfully prepared a stable ambipolar perfluoroporphyrin-based polymeric film by electrochemical synthesis. Our strategy involved the synthesis of a novel tetra-pentafluorophenyl porphyrin covalently linked to four 3,4-ethylenedioxythiophene (EDOT) moieties. The resulting monomer, **EDOT-TPPF$_{16}$**, was obtained through a straightforward synthetic approach with a good overall yield. The unique molecular structure of **EDOT-TPPF$_{16}$** serves a dual function, with EDOT moieties allowing electropolymerization for polymeric film formation, while the electron-acceptor porphyrin core enables electrochemical reduction and electron transport. The electrochemical polymerization permits the polymer (**PEDOT-TPPF$_{16}$**) synthesis and film formation in a reproducible and controllable manner in one step at room temperature. Spectroelectrochemical experiments confirmed that the porphyrin retained its optoelectronic properties within the polymeric matrix after the electrochemical polymerization. The obtained polymeric material exhibited stable redox capabilities. Current charge–discharge cycles and electrochemical impedance spectroscopy of the electrochemically generated organic film demonstrated that the polymer could be applied as a promising active material in the development of supercapacitor energy storage devices.

Received 5th February 2024
Accepted 29th April 2024

DOI: 10.1039/d4ra00945b

rsc.li/rsc-advances

1. Introduction

Structures based on porphyrins hold significant biological and technical importance as they have crucial roles in light absorption, oxygen transportation, redox reactions, and electron transfer processes.[1,2] Porphyrins possess exceptional characteristics, including optical, magnetic, redox, and photophysical properties, making them highly valuable for a wide range of applications. Chemically modified porphyrins with different functionalities can be tailored for use in solar cells,[3,4] sensors,[5,6] medical imaging,[7,8] photodynamic therapy,[9–11] supercapacitors,[1,12,13] and other applications. Porphyrins are characterized by their highly stable aromatic macrocyclic nature, abundant nitrogen atoms, and an extensive π-conjugated system. In recent years, research on organic polymers based on aromatic macrocycles has shown rapid and diverse advancements.[14–17] In particular, porphyrin-based polymers have received considerable attention because these polymers usually retain the original outstanding optical and electrical properties of the constituent porphyrin monomers, as well as their structural adaptability.[18] These polymers are widely used in diverse fields, such as energy storage,[19,20] adsorption,[16,21] separation,[16,17] sensing,[22] and optoelectronics,[23,24] among others. Specially designed porphyrin monomers can be used to produce polymers with highly branched structures, primarily through modifications at the four *meso* positions with polymerizable groups.[25,26] Tetradentate porphyrin-based polymers can improve substance transport through the void spaces in the polymeric matrix.[21] Additionally, porphyrin-based conducting polymers can be designed for diverse purposes for the development of electronic and optoelectronic devices, as either

[a]*IITEMA-CONICET, Departamento de Química, Facultad de Ciencias Exactas, Físico-Químicas y Naturales, Universidad Nacional de Río Cuarto, Agencia Postal Nro. 3, X5804BYA Río Cuarto, Córdoba, Argentina. E-mail: mgervaldo@exa.unrc.edu.ar; Fax: +54 358 76233; Tel: +54 358 4676538*

[b]*IDAS-CONICET, Departamento de Química, Facultad de Ciencias Exactas, Físico-Químicas y Naturales, Universidad Nacional de Río Cuarto, Agencia Postal Nro. 3, X5804BYA Río Cuarto, Córdoba, Argentina. E-mail: dheredia@exa.unrc.edu.ar*

[c]*INFIQC-CONICET, Departamento de Química Orgánica, Facultad de Ciencias Químicas, Universidad Nacional de Córdoba, Córdoba X5000HUA, Argentina*

[d]*INTEMA-CONICET, Facultad de Ingeniería, Universidad Nacional de Mar del Plata, B7606WV Mar del Plata, Buenos Aires, Argentina*

† Electronic supplementary information (ESI) available. See DOI: https://doi.org/10.1039/d4ra00945b

‡ These authors contributed equally to this work.

hypercrosslinked fully conjugated polymers or non-conjugated redox polymers.[16,27,28]

Powdered polymers derived from porphyrins can exhibit high porosity and a crystalline structure; however, they are often difficult to manage and dissolve, limiting their practical applications. Traditional coating techniques such as spin coating, dip coating, or layer-by-layer self-assembling encounter challenges in creating uniform films from these powdered porphyrin polymers. Additionally, chemical polymerization typically involves complex or multi-step procedures and challenging purification steps due to low solubility.[29,30] An innovative approach to face this situation is to incorporate electropolymerizable groups into porphyrin macrocycles. These moieties participate in electrochemically induced coupling reactions, producing novel polymeric materials with connected macrocycles.[31,32] Electrochemical methods enable the direct polymer synthesis and the fabrication of polymeric films on conductive substrates in a single step, circumventing the challenges associated with the use of polymer powders obtained from chemical polymerization.[33] Electrochemical polymerization is a versatile methodology used to create organic films over metallic contacts or transparent conducting oxides. The electrochemical process is simple, reproducible, and has clear advantages over chemical polymerization and other deposition techniques. Depending on the electrochemical method used, it is possible to achieve precise control over film thickness.[34–36] Similarly, the morphology of the resultant films can be tailored by adjustment of the experimental conditions and electrochemical parameters.[36–38] Unlike chemical synthesis, electropolymerization is a one-step process, eliminating the need for subsequent purification as only the monomer is present in the solution. There is also a significant reduction in waste production.[39] In addition, electropolymerization is conducted at room temperature, providing an advantage over thermal evaporation methods that require materials with high thermal stability. In many cases, polymers tend to decompose before reaching the sublimation stage in the thermal evaporation processes.

On the other hand, currently, many reports related to the development of organic functional materials[40] involve the synthesis of new compounds through complex synthetic pathways that require multiple steps, high-cost reagents, complex reaction conditions, and/or reactions that result in low yields. Although these processes frequently produce materials with remarkable properties that are essential for the advancement of state-of-the-art technologies,[41–43] it is critical to recognize the difficulties associated with this situation. Practical implementation, large-scale production, and commercialization of the reported materials may be hindered, impeding the transition from laboratory to marketplace. Consequently, in pursuit of practical applications, there is a pressing need to pivot toward more straightforward, cost-effective synthetic approaches that take into account both scalability and feasibility. In response to this demand, we have developed a simple synthetic procedure of two steps for the monomeric tetradentate porphyrin that utilizes readily accessible, affordable, and commercially available starting materials.

In this work, we report for the first time the monomer synthesis of a tetra-ethylenedioxythiophene (EDOT) modified fluorinated porphyrin (**EDOT-TPPF$_{16}$**) and the subsequent electrochemical synthesis of polymeric films (**PEDOT-TPPF$_{16}$**). The design of this monomer combines the highly robust perfluorinated porphyrin, which has extraordinary photo and chemical stability, with the versatile and widely used electropolymerizable EDOT group, which is an adaptable matrix to generate electrodeposited polymers that show excellent stability and redox properties.[44–46] The presence of fluorine atoms in the porphyrin macrocycle is known to enhance photostability, influence redox characteristics, and increase singlet oxygen generation.[47,48] In this sense, fluorinated porphyrin-based polymers have been utilized as oxygen carriers to enhance photodynamic therapy, particularly in alleviating tumor hypoxia.[47,49,50] Additionally, perfluorinated porphyrins have found applications in developing active materials for oxygen sensing,[51,52] and fluorinated porous conjugated polyporphyrins were applied in heterogeneous catalysis.[53] The electrochemical polymerization of **EDOT-TPPF$_{16}$** led to the synthesis and deposition of electroactive polymeric films that were characterized by UV-visible spectroscopy, cyclic voltammetry (CV), atomic force microscopy (AFM), scanning electron microscopy (SEM) and spectroelectrochemistry. **PEDOT-TPPF$_{16}$** films were evaluated as pseudocapacitive polymers through galvanostatic charge–discharge (GCD) experiments and electrochemical impedance spectroscopy (EIS). Our outcomes showed that these polymeric films are promising materials that can be used in energy storage devices. To the best of our knowledge, this work represents the first electropolymerization of a perfluorinated porphyrin substituted with EDOT, showcasing promising and potential optoelectronic properties.

2. Experimental section

2.1. Synthesis

2.1.1. Synthesis of TPPF$_{20}$. 2,3,4,5,6-Pentafluorobenzaldehyde (1.50 g, 7.65 mmol) was dissolved in dichloromethane (DCM, 320 mL), and then pyrrole (552 μL, 7.96 mmol) was added. The solution was purged with a pure argon stream for around 15 minutes to remove the air. Afterward, $BF_3 \cdot OEt_2$ (118 μL, 0.96 mmol) was dropwise added, and the mixture was stirred at room temperature (r.t.) for 44 h under argon atmosphere. After that, 2,3-dichloro-5,6-dicyano-1,4-benzoquinone (DDQ) (1.38 g, 6.08 mmol) was added, and the resulting solution was stirred at room temperature for another 2 h. The solution was concentrated under reduced pressure until the volume was reduced by approximately half, after which it was passed through a short silica pad. The organic solvent was removed *in vacuo*, and the crude product was purified by chromatography (silica gel, hexane/DCM, 7 : 3) to give the desired macrocycle **TPPF$_{20}$** (1.25 g, 1.28 mmol, 67%) as a purple solid. The NMR data for this porphyrin were consistent with the literature. ^{1}H NMR (500 MHz, $CDCl_3$) δ 8.92 (s, 8H, pyrrole-H), −2.91 (s, 2H, pyrrole N–H). ^{19}F NMR (500 MHz, $CDCl_3$) δ −136.44 to −136.56 (m, 8F), −151.21 (t, J = 20.8 Hz, 4F), −161.32 (td, J = 22.7, 7.5 Hz, 8F).

2.1.2. Synthesis of EDOT-TPPF$_{16}$. **TPPF$_{20}$** (450 mg, 0.46 mmol) and hydroxymethyl EDOT (EDOT-OH, 396 mg, 2.30 mmol) were dissolved in anhydrous *N*,*N*-dimethylformamide (DMF, 50 mL) and purged with argon. Subsequently, Cs_2CO_3 (6.19 g, 19.0 mmol) was added, and the mixture was purged with argon for an additional 5 minutes. The resulting mixture was then heated at 100 °C for 1 hour. Afterward, the reaction was allowed to cool to room temperature and was diluted with DCM. The solution was washed with water thrice, and the solvent from the green organic phase was removed under reduced pressure. The crude product was purified by chromatography column (silica gel, DCM/hexane, 9 : 1) to afford the desired product **EDOT-TPPF$_{16}$** (539 mg, 0.34 mmol, 74%). ^{1}H NMR (500 MHz, $CDCl_3$) δ 8.91 (s, 8H), 6.49 (d, J = 3.6 Hz, 4H), 6.47 (d, J = 3.6 Hz, 4H), 4.85–4.81 (m, 4H), 4.81–4.73 (m, 8H), 4.54 (d, J = 12.0 Hz, 4H), 4.46 (dd, J = 11.7, 6.2 Hz, 4H), −2.90 (s, 2H). ^{19}F NMR (500 MHz, $CDCl_3$) δ −138.01 (dd, J = 21.2, 5.8 Hz, 8F), −156.71 (dd, J = 22.3, 7.5 Hz, 8F). MALDI-TOF [m/z] 1583.172 $[M + H]^+$ (1583.119 calculated for $C_{72}H_{39}F_{16}N_4O_{12}S_4$).

2.2. Spectroscopic properties

The UV-visible absorption spectra of **EDOT-TPPF$_{16}$** and **PEDOT-TPPF$_{16}$** were obtained in a diluted acetonitrile (ACN) solution and a thin film electrodeposited on indium tin oxide (ITO), respectively. The spectrum of **EDOT-TPPF$_{16}$** was recorded and compared with that of **TPPF$_{20}$** at room temperature using a quartz cuvette with a 10 mm path. The absorption spectrum corresponding to **PEDOT-TPPF$_{16}$** on ITO was acquired by placing the electrode in the spectrometer cell holder. For background correction, a bare ITO electrode was utilized. Fluorescence emission spectra of **EDOT-TPPF$_{16}$** and **TPPF$_{20}$** were recorded in diluted ACN solutions at room temperature, exciting the sample at the maximum of the Soret band (Abs = 0.1).

2.3. Electrochemistry and electrodeposition

2.3.1. Chemicals for electrochemical experiments. ACN and 1,2-dichloroethane (DCE), both anhydrous solvents, were obtained from Sigma-Aldrich Co. and used as received. Tetrabutylammonium hexafluorophosphate ($TBAPF_6$) and tetrabutylammonium perchlorate (TBAP), both salts for electrochemical analysis, were purchased from Sigma-Aldrich Co. and used without further purification.

Electrochemical measurements were carried out as described previously.[26,35,54,55] CV, differential pulse voltammetry (DPV), GCD tests, and EIS were performed at room temperature with a Palm Sense 4 potentiostat. Electrochemical studies were performed in a deaerated (with high purity argon) monomer solution containing 0.1 M of the supporting electrolyte or only with electrolyte—the last solution for the electrochemical responses of the electropolymerized films. A three-electrode system composed of a glassy carbon (GC) or ITO coated glass working electrode, a platinum wire counter electrode, and a silver wire quasi-reference electrode were utilized for electrochemistry experiments. Ferrocene was used as internal standard for reference potential calibration in organic media (*vs.* Saturated Calomel Electrode, SCE). Fc/Fc^+ = 0.40 V *vs.* SCE.[36] The ITO electrode substrates (Delta Technologies, nominal resistance 8–12 Ω per square) were cleaned sequentially in an ultrasonic bath with acetone, ethanol, and deionized water and dried before use.

The quantification of the electropolymerized material on the ITO electrode was determined following the methodology outlined by Zhang *et al.* and other researchers.[56] This method assumes that, after electropolymerization, any alterations in the absorption coefficient of the porphyrin chromophore are negligible.[26] Adopting the above-mentioned methodology ensures a reliable estimation of the quantity of electropolymerized material by considering the minimal changes in the absorption characteristics of the porphyrin chromophore.

2.4. X-ray diffraction (XRD)

XRD scanning of **PEDOT-TPPF$_{16}$** electrodeposited on ITO was measured using a Panalytical X'Pert PRO X-ray Diffractometer (30 mA and 40 kV) equipped with a Cu-Kα radiation source ($\lambda \sim$ 1.54 Å) at room temperature. The scans were performed in a 2θ range of 10–60° at 1° min^{-1}.

2.5. Fourier transform infrared spectroscopy (FTIR)

FTIR spectroscopic analysis of **EDOT-TPPF$_{16}$**, and **PEDOT-TPPF$_{16}$** was performed in attenuated total reflectance mode (ATR-FTIR) using a Nicolet 6700, Thermo Scientific Inc. device. Spectra were recorded in the range of 400–4000 cm^{-1}, performing 64 scans with a resolution of 4 cm^{-1} at room temperature.

2.6. Spectroelectrochemical studies

Spectroelectrochemical measurements were carried out as described previously.[35,57] *In situ* UV-visible spectroelectrochemical measurements under potentiostatic control were obtained using a Hewlett Packard UV-vis diode array spectrophotometer at kinetic measurement mode by utilizing a three-electrode configuration of an ITO modified with polymeric film (see Fig. S1†). A naked ITO electrode was used as a blank for absorption background correction.

2.7. Surface characterization

2.7.1. Scanning electron microscopy. SEM images were captured utilizing a field emission scanning electron microscope (FE-SEM), specifically the Sigma Zeiss model. The acceleration voltage was set at 5 kV, and the signal was recorded using an in-lens detector, while maintaining a working distance of 4 mm. The samples were previously coated with a thin layer of gold to prevent charging and mitigate material deterioration.

2.7.2. Atomic force microscopy. AFM measurements were conducted using an Agilent Technologies SPM/AFM microscope model 5500. The samples were scanned using intermittent contact, specifically employing the Acoustic AC Mode. Silicon cantilevers (Budget Sensors, TAP 150 AI-G) with a spring constant of approximately 5 N m^{-1} and a resonant frequency of around 150 kHz were utilized. Images were acquired by

adjusting the oscillation frequencies of the cantilevers to be slightly below their resonant frequencies. The scanning speed was set at 0.45 lines per second. Topographical images were generated from raw data values processed and analyzed using the Gwyddion 2.62 software package.

2.8. GCD and EIS measurements

In order to evaluate the performance of the porphyrin films as supercapacitive materials, GCD and EIS experiments were carried out in a three-electrode configuration using a GC working electrode modified with polymeric film, in TBAP/ACN solution.

GCD-test was performed over a cell cycled between 0–(+1.0) and 0–(−1.0) V at various current densities with chronopotentiometry method. Before and after charge–discharge experiments, **PEDOT-TPPF$_{16}$** film was evaluated by CV in the supporting electrolyte solution until obtained repetitive profiles.

The specific capacitance was calculated with respect to the mass of the activated polymeric material using eqn (1).

$$C(\mathrm{F\ g^{-1}}) = \frac{I}{\mathrm{d}E/\mathrm{d}t} \quad (1)$$

where C, I and $\mathrm{d}E/\mathrm{d}t$ are the gravimetric capacitance, discharging current per mass unit applied to the electrode and the slope during the voltage drop in the GCD experiment, respectively.[58]

EIS was performed using a range of 0.1–10^5 Hz with a perturbation amplitude of 5 mV at an applied potential of 0.75 V.[59,60]

3. Results and discussion

3.1. Design, synthesis, and characterization of EDOT-TPPF$_{16}$ monomer

As mentioned above, the development of simple synthetic processes is paramount for advancing materials used in the field of optoelectronics. The implementation of organic materials in real practical applications necessitates a transition to less complex and more economical synthetic procedures. Thus, we implemented a straightforward two-step synthesis approach, utilizing readily accessible and affordable initial materials.

The synthesis of **EDOT-TPPF$_{16}$** was carried out as shown in Scheme 1. The first step involved an acid-catalyzed condensation reaction between pyrrole and pentafluorobenzaldehyde in DCM at room temperature for 44 hours. After this period, the hydrogenated tetrapyrrolic macrocycle was oxidized with DDQ in a one-pot reaction, affording the tetra-aryl porphyrin **TPPF$_{20}$** with a good yield of 67%.[61] This macrocycle is a versatile building block that can be used to construct more complex and elaborated materials by attaching additional moieties with the desired properties.[62–64] Pentafluorophenyl (PFP) groups located around the porphyrin ring can be regioselectively functionalized with a wide range of nucleophiles (alcohols, azide, thiols, amines, *etc.*) through nucleophilic aromatic substitution (S_NAr) reactions.[61–65]

In a second step, the fluorinated template **TPPF$_{20}$** was subjected to a regioselective S_NAr with EDOT-OH. For this kind of transformation using alcohols, it is common to employ KOH in dry tetrahydrofuran, using an excess of alcohol to avoid the formation of hydroxide.[65] However, we opted for different conditions. The functionalization of the flexible matrix **TPPF$_{20}$** was carried out in DMF and using Cs_2CO_3.[66] Thus, after one hour of reaction, the alcohol was converted into the alkoxide, and the substitution of the four *para*-fluoro atoms of the PFP groups occurred. The EDOT-substituted porphyrin (**EDOT-TPPF$_{16}$**) was obtained with yields as high as 74% and good reproducibility.

The molecular structure of **EDOT-TPPF$_{16}$** was fully elucidated and determined by Fourier-transform infrared spectroscopy (FT-IR), nuclear magnetic resonance (NMR) spectroscopy, and matrix assisted laser desorption ionization – time of flight (MALDI-TOF) spectrometry (Fig. S2–S8†). The tetrasubstituted tetrapyrrolic macrocycle was confirmed in the first instance by MALDI-TOF, which disclosed the incorporation of the four EDOT moieties. The ^{1}H NMR spectrum of **EDOT-TPPF$_{16}$** combined the characteristic resonances of the EDOT unit, together with the diagnostic protons corresponding to the porphyrin ring. In the aromatic region, due to the symmetric substitution of the tetrapyrrolic macrocycle, the eight β-pyrrolic protons gave rise to a singlet at $\delta = 8.91$ ppm. The thiophene protons appeared as two doublets at $\delta = 6.49$ and $\delta = 6.47$ ppm ($J = 3.6$ Hz) due to the asymmetric substitution on the EDOT ring. The integrals of these two signals were four each, confirming the incorporation of four EDOT units, and consistent with the cruciform architecture of the porphyrin-core. In the aliphatic region, the methylene and methine resonances belonging to the dioxin ring are overlapped in the region between 4.40 and 4.90 ppm, giving rise to complex multiples. Finally, in the upfield region, a singlet at $\delta = -2.90$ ppm that integrated for two is assigned to the inner NH protons of the macrocycle. On the other hand, ^{19}F spectrum of **EDOT-TPPF$_{16}$** was used not only to confirm the tetra-substitution but also to demonstrate the regioselectivity of the S_NAr. The spectrum of the tetra-substituted porphyrin exhibits a complete disappearance of the triplet at $\delta = -151.21$ ppm corresponding to the *para*-fluorine atoms. Furthermore, the doublet belonging to *meta*-fluorine atoms exhibits a shift from $\delta = -161.32$ ppm in **TPPF$_{20}$** to $\delta = -156.71$ ppm in **EDOT-TPPF$_{16}$**. These fluorine atoms near the nucleophile are more sensitive than the doublet in the *ortho* position, which only presents a slight shift.[66]

At this point, we synthesized a *meso*-pentafluorophenyl-substituted tetrapyrrole system that combines an electron-withdrawing porphyrin core with four electropolymerizable EDOT moieties in the periphery. We chose the **TPPF$_{20}$** nucleus because the highly robust perfluorinated porphyrin exhibits extraordinary chemical stability, water repulsion properties, and undergoes two reversible reduction processes.[61,67,68] The attachment of EDOT moieties into this macrocycle offers an innovative approach to participate in electrochemical coupling reactions, creating a new polymeric material with interconnected porphyrin cores. EDOT polymers are characterized by their electrochemical stability, ultrafast electron-transfer

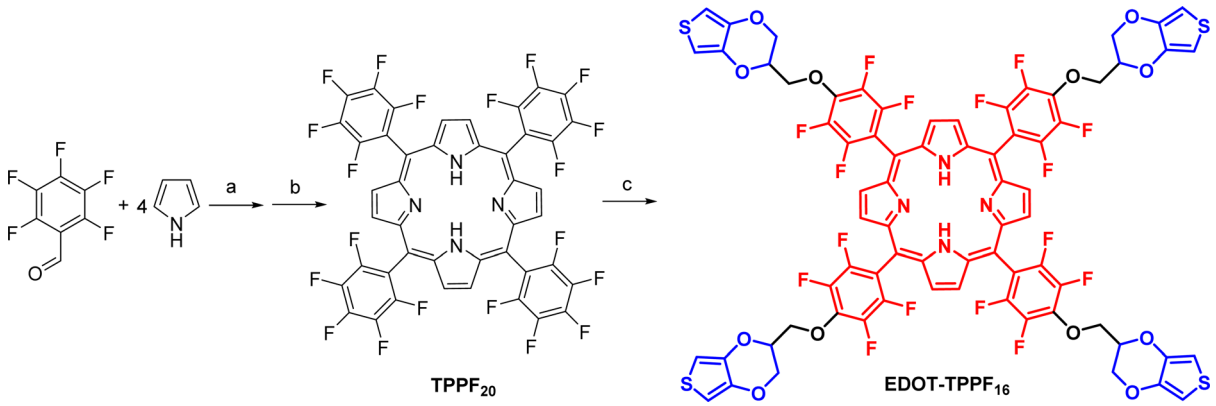

Scheme 1 Synthesis of **EDOT-TPPF$_{16}$**. Reagents and conditions: (a) $BF_3{\cdot}OEt_2$, DCM, r.t., 44 h; (b) DDQ, DCM, r.t., 1.5 h, 67%; (c) EDOT-OH, DMF, Cs_2CO_3, 70 °C, 4 h, 74%.

rates, and good hole-transporting and capacitive properties.[45,46] Thus, EDOT units in **EDOT-TPPF$_{16}$** can be employed for the electrochemical production of polymeric films directly onto conductive substrates in a single step, with the porphyrin core serving as the n-type material and the **PEDOT** chain as the p-type material.

3.2. Electrochemical characterization of EDOT-TPPF$_{16}$

Comparative electrochemical studies of **TPPF$_{20}$** and **EDOT-TPPF$_{16}$** were carried out using CV and DPV measurements in order to determine their electrochemical properties. The analysis was performed on GC (Fig. 1a and b). **TPPF$_{20}$** CV presents two quasireversible oxidations (DPV peaks at 1.38 and 1.63 V *vs.* SCE) and two quasireversible reductions (DPV peaks at −0.89 and −1.31 V *vs.* SCE). These results are typical for free base porphyrins, which usually show two well-defined reversible single-electron macrocycle oxidations and reductions in nonbinding solvents,[69] related to the formation of the corresponding radical cation and dication, and radical anion and dianion, respectively.[70–72] However, it is known that peripheral substitution in tetraphenyl porphyrins has a strong effect in modulating their electron donor–acceptor capabilities. In the present case, we observed that the **TPPF$_{20}$** oxidation occurs at more positive (anodic) and the reduction at less negative (cathodic) potentials compared to the values reported for tetraphenyl porphyrins without substituents. This is a consequence of the electron-withdrawing effects characteristic of the perfluorinated benzene rings.[69,70] On the other hand, **EDOT-TPPF$_{16}$** exhibits similar quasireversible reductions but only one irreversible oxidation peak at around 1.25 V (cyan voltammogram in Fig. 1a), with a peak current value around four times higher than the first reduction peak. It is known that EDOT is oxidized at around 1.2 V *vs.* SCE, showing an irreversible peak in the first anodic scan;[73,74] thus, the irreversible redox process can be assigned to oxidation of the four EDOT units bounded to the macrocycle in **EDOT-TPPF$_{16}$**.

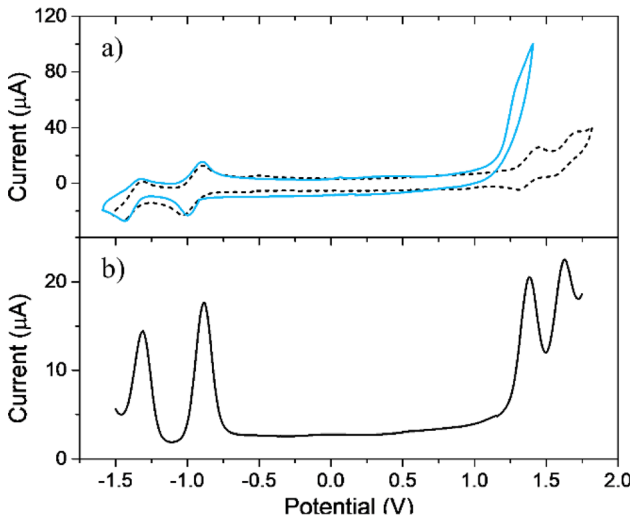

Fig. 1 (a) Cyclic voltammograms of TPPF$_{20}$ (black dashed line) and EDOT-TPPF$_{16}$ (cyan continuous line) in a solution of DCE containing supporting electrolyte (TBAPF$_6$, 0.1 M). GC electrode, scan rate 0.100 V s^{-1}. (b) DPV of TPPF$_{20}$ clearly exhibiting the four redox processes.

3.3. Electrodeposition of PEDOT-TPPF$_{16}$ polymeric film

It is well-known that upon oxidation EDOT and its derivatives give rise to unstable radical cations that subsequently react to produce EDOT dimers, exhibiting these dimers easier oxidations than the corresponding EDOT monomers.[54,75] Furthermore, EDOT dimers, trimers, and oligomers have the potential to undergo radical coupling, leading to the formation of PEDOT chains (Scheme S1†). Fig. 2a shows twenty repetitive CV anodic scans for **EDOT-TPPF$_{16}$** in the −0.30 to 1.25 V potential range, where increments in the oxidation–reduction currents are detected with each new cycle, typical of the growing of an electroactive film over the GC electrode.[75–77] To confirm the formation of a film, the electrochemical response of the electrode was obtained in a solution containing only supporting electrolyte (Fig. 2b). The electrochemical response of **PEDOT-TPPF$_{16}$** film is characterized by the presence of two reduction processes (−0.85 and −1.40 V) and one broad oxidation between 0.20 and 1.10 V with a peak potential at around 0.50 V (Table 1). The two redox systems at negative potentials can be

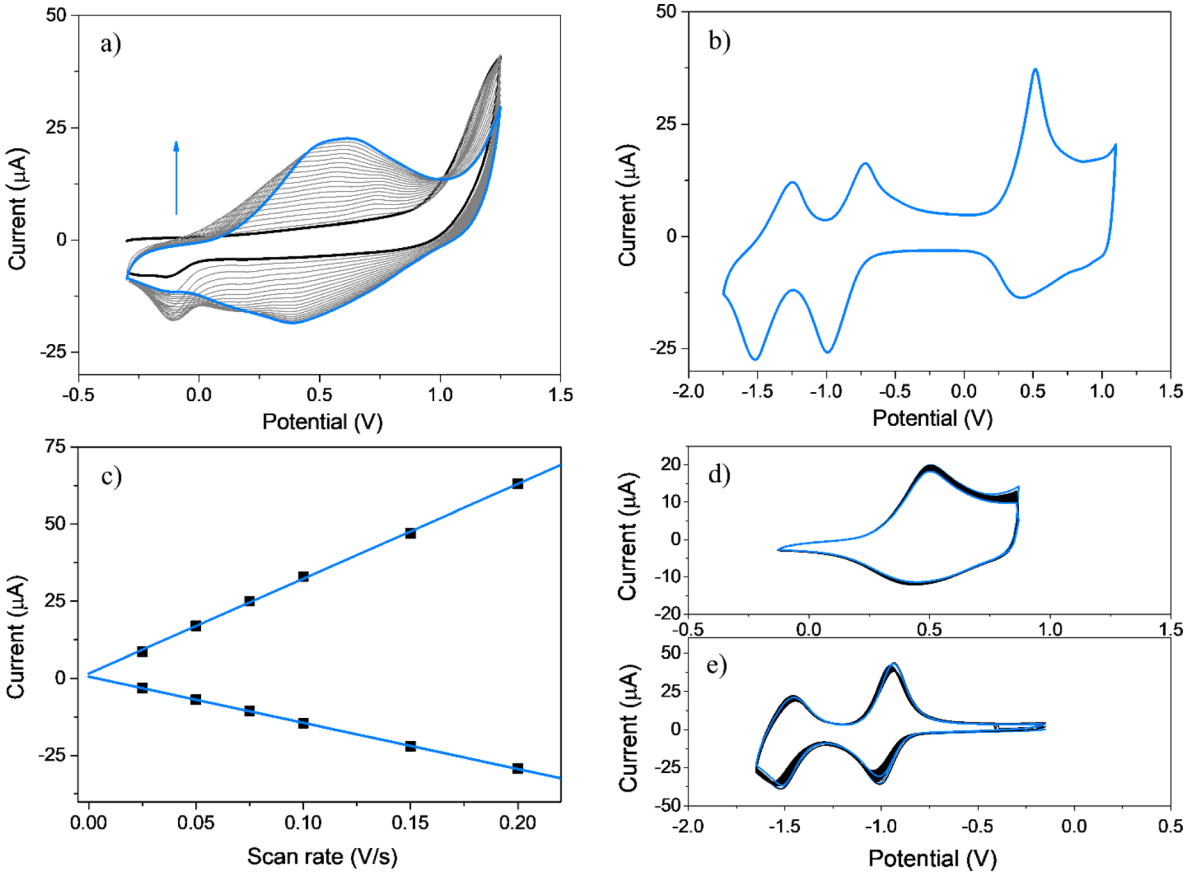

Fig. 2 (a) First (black), 2nd–19th (grey) and 20th (cyan) cyclic voltammograms of **EDOT-TPPF$_{16}$**. Scan rate: 0.100 V s^{-1}. The measurements were done in DCE containing TBAPF$_6$ using a CG working electrode. (b) Electrochemical response of the electropolymerized film **PEDOT-TPPF$_{16}$** at 0.100 V s^{-1}. (c) Relationship between the peak currents *vs.* different scan rates (0.025, 0.050, 0.075, 0.100, 0.150, 0.200 V s^{-1}). Data were taken at the potentials of the oxidation and reduction peaks of (b). (d and e) One hundred CV cycles of the film for: (d) oxidation and (e) reduction processes. Scan rate 0.100 V s^{-1}, cyan lines: first and 100th cycle. (b–e) In ACN containing only support electrolyte (TBAP).

associated with the reductions of the porphyrin macrocycle, generating the corresponding radical anion and dianion.[69–72] The broad oxidation can be due to the oxidation of new EDOT dimer, trimer, or long chains which were formed by the coupling of EDOT radical cations, generated during continuous cycling.[75,76] Superimposed in this broad oxidation might be also involved the oxidation of the porphyrin macrocycle.[70,73] A similar electrochemical response has been reported for a film obtained after electropolymerization of a EDOT-trimer mono substituted porphyrin monomer.[78] The peak currents for the redox systems present a linear relationship with the scan rate (Fig. 2c), which indicates an electroactive product irreversibly adsorbed over the electrode surface. The assessment of the stability of the polymeric material during oxidation and

Table 1 Spectroscopic properties, redox potentials of **TPPF$_{20}$**, **EDOT-TPPF$_{16}$** monomer and **PEDOT-TPPF$_{16}$** electrodeposited polymer. Conditions: DCE/0.10 M TBAPF$_6$, scan rate = 0.100 V s^{-1}

	Wavelength (nm)					Potentials[d]			
						Oxidation		Reduction	
Compound	Soret	Q_I	Q_{II}	Q_{III}	Q_{IV}	I	II	I	II
TPPF$_{20}$	406[c]	634[c]	580[c]	534[c]	503[c]	1.38[e]	1.63[e]	−0.89[e]	−1.31[e]
PEDOT-TPPF$_{16}$	415	643	589	546	509	0.60[a] 0.50[b]	—	−1.00[a] −0.85[b]	−1.55[a] −1.4[b]
EDOT-TPPF$_{16}$	410[c]	635[c]	583[c]	538[c]	504[c]	1.25[a]	—	−1.00[a] −0.94[b]	−1.45[a] −1.37[b]

[a] Peak potential. [b] Half wave potential. [c] Solution in ACN. [d] Potential *vs.* SCE. [e] DPV potentials.

reduction processes was evaluated through the application of continuous CV cycles. Fig. 2d and e show one hundred superimposed cycles for both oxidation and reduction processes, respectively. The noteworthy outcome is the absence of any substantial evidence indicating a marked decrease in the current values over the cycles. This observation shows that the organic material remains resilient, exhibiting no signs of dissolution or structural alterations throughout the CV, thereby maintaining its electrochemical activity intact.

3.4. Characterization of the ambipolar polymeric film. Spectroscopic properties

Spectroscopic and spectroelectrochemical experiments were conducted to verify the formation of the films, investigate their electro-optical properties, and thoroughly analyze the reversibility linked to the redox processes. Specifically, these experiments were carried out by depositing **PEDOT-TPPF$_{16}$** films onto semitransparent ITO electrodes. This experimental setup allowed a detailed exploration of the characteristics and behaviors of the films, offering valuable insights into their electrochemical and optical responses. The semitransparent nature of the ITO electrodes facilitated the examination of the changes in the electronic spectra of the organic polymer in response to electrochemical stimuli. The formation of **PEDOT-TPPF$_{16}$** film on ITO electrode was performed by applying repetitive CV anodic scans for **EDOT-TPPF$_{16}$** in DCE-TBAPF$_6$ (Fig. 3a). It can be seen that during anodic cycling, increases in oxidation–reduction currents are detected, indicating the formation and deposition of the film over the oxide semiconductor. This is a non-trivial result, as the nature of the electrode is changed. The voltammetric response of the electrode (Fig. 3b) is similar to that obtained on GC electrode (Fig. 2b), which presents two redox systems at negative potential values and a broad oxidation. In this case, the peak currents for the redox systems are also linear with the scan rate, confirming the formation of a film over the ITO electrode.

Photophysical properties of **EDOT-TPPF$_{16}$** monomer and **PEDOT-TPPF$_{16}$** electrodeposited polymer were studied and compared in diluted solution and thin solid films, respectively. Fig. 4 displays UV-visible absorption spectra of **EDOT-TPPF$_{16}$** in ACN solution and **PEDOT-TPPF$_{16}$** electrode obtained by placing it in the spectrometer cell holder, both at room temperature. The main absorption characteristics are presented in Table 1. The monomer **EDOT-TPPF$_{16}$** presents the characteristic spectrum of symmetrical free base porphyrin, with a strong absorption in the blue region that belongs to the Soret band ($\lambda_{max} = 410$ nm). Additionally, the four characteristic Q bands of the substituted porphyrin are observed in the red region (between 500 and 650 nm).[61,79] The sharp electronic transition for the Soret band indicates that the monomer is not aggregated in that solvent. Furthermore, it is worth mentioning that the absorption spectrum of **EDOT-TPPF$_{16}$** closely resembles that of **TPPF$_{20}$** (see Fig. 4). The Soret band of **EDOT-TPPF$_{16}$** exhibits a slight bathochromic shift of ~4 nm, which is a consequence of the auxochromic effect generated by the oxy substituents.[65,66] These outcomes disclose that the external substitution of the

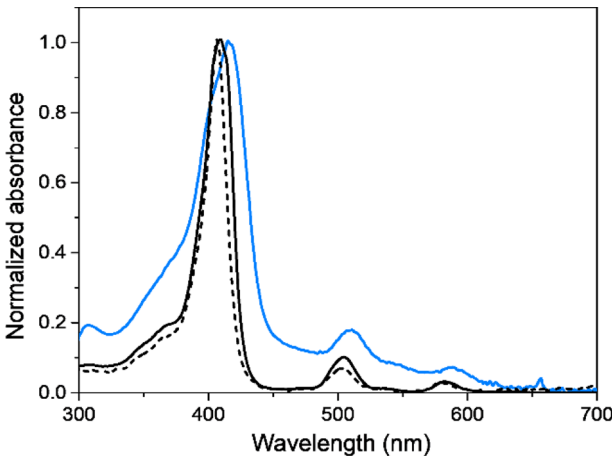

Fig. 4 Absorption spectra of TPPF$_{20}$ (black dashed line), EDOT-TPPF$_{16}$ monomer (black continuous line) in ACN and PEDOT-TPPF$_{16}$ electrodeposited polymer on ITO (cyan continuous line).

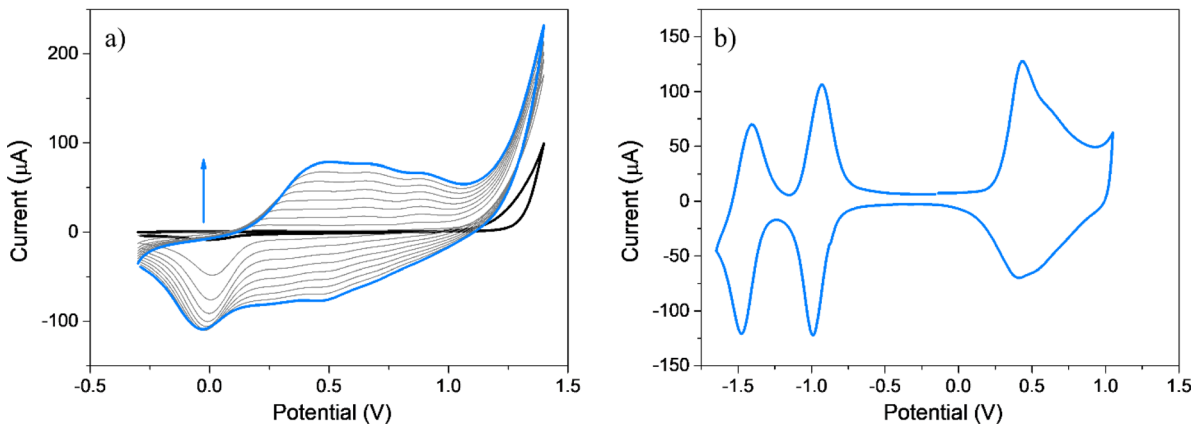

Fig. 3 (a) First (black), 2nd–9th (grey) and 10th (cyan) cyclic voltammograms of EDOT-TPPF$_{16}$. The measurements were done in DCE containing TBAPF$_6$ (0.1 M) using an ITO working electrode. (b) Electrochemical response of the electropolymerized film PEDOT-TPPF$_{16}$ in ACN containing only TBAP (0.1 M). Scan rate: 0.100 V s^{-1}.

PFP groups does not significantly affect the porphyrin-based chromophore. Similarly, the fluorescence emission spectra of **TPPF$_{20}$** and **EDOT-TPPF$_{16}$** in ACN presented a close resemblance (Fig. S9†). Both compounds exhibited the characteristic red fluorescence emission of the pentafluorophenyl-substituted porphyrins, with two emission bands centered around 635 and 700 nm.[61,79]

Regarding the **PEDOT-TPPF$_{16}$** polymer, the UV-visible absorption spectrum exhibits similar spectroscopic features to the monomer **EDOT-TPPF$_{16}$**, revealing that the optical properties of the porphyrin-based chromophore are conserved in the polymeric chain. As it can be observed, the electronic transitions corresponding to the tetrapyrrolic macrocycle are clearly defined. The electronic transitions of the porphyrin in the polymer resemble those of the monomer in solution, with well-defined Soret and Q bands. This result not only validates the presence of tetrapyrrolic macrocycle in the film but also demonstrates that the molecular structure of the porphyrin core is maintained intact throughout the electrodeposition process. It is worth noting that there is a broadening and a slight red-shift of the bands of approximately 5 nm compared to the monomer **EDOT-TPPF$_{16}$** in solution, indicating a weak interaction of the porphyrin cores in the polymeric chain. This is not trivial data since the solid state represents a highly aggregated system.

XRD experiment conducted for **PEDOT-TPPF$_{16}$** reflects an amorphous nature of the obtained material (Fig. S10†). This result agrees with PEDOT-based polymeric materials in literature, where a broad diffraction halo is reported at *ca.* 25°.[80–82] This could be indicative of interchain planar ring stacking of the polymer. Additionally, low peaks can be found due to the presence of the electrolyte, but they do not correspond to the **PEDOT-TPPF$_{16}$** structure. In order to get more information about the polymerization mechanism and the chemical structure of the polymer, FT-IR spectra of **EDOT-TPPF$_{16}$** monomer and **PEDOT-TPPF$_{16}$** film were obtained (Fig. S11†). It can be seen that **EDOT-TPPF$_{16}$** monomer presents two bands at around 1184 and 891 cm^{-1}, associated with =C–H in-plane and out-of-plane deformation vibrations of the EDOT units, while these bands are absent in the spectra of **PEDOT-TPPF$_{16}$** film. The disappearance of these two peaks indicates an efficient coupling of the EDOT units through the α positions, which supports the proposed polymerization mechanism.[83]

3.5. Spectroelectrochemical characterization

As already mentioned, spectroelectrochemical studies allow us to obtain information about the chemical structure of the polymer and the redox species involved during the oxidation and reduction processes. The spectra at the different applied potentials were plotted as ΔAbs (subtracting the absorption spectrum at 0.00 V) and are shown in Fig. 5a and b. When the film is oxidized, at applied potentials between 0.00 and 0.40 V, no changes are observed, while at more positive values, the bleaching of the Soret band and two new positive bands at around 440 and 630 nm are detected. The observed spectral changes are predominantly originated from changes in the porphyrin nucleus present in the polymer. Moreover, the observation of clear isosbestic points evidently shows that the formed species are generated by oxidation of the tetrapyrrolic ring, meanwhile the full reversibility of the obtained spectra after film reduction is in agreement with the stable electrochemical response observed after hundreds of successive CV cycles. The new absorption band developed during oxidation agrees with the presence of porphyrin radical cation in the polymeric film (Fig. 5a).[84,85] On the other hand, a similar spectroelectrochemical response is observed in the negative potential range (Fig. 5b). Before the film is reduced (0.00 and −0.80 V), there are no changes in the absorption values, but at more negative applied potentials, two new positive bands appear around 440 and 570 nm, accompanied by the bleaching of the Soret band. The absorption bands developed during the reduction processes are comparable to those reported and assigned to the radical anion of the porphyrin macrocycle.[86] Therefore, considering the electrochemical, spectral, and spectroelectrochemical data, it is possible to confirm the unaltered presence of the porphyrin macrocycle as photoactive and electroactive centers embedded in the polymeric matrix. The porphyrins are covalently bonded to each other by EDOT dimers, trimers, or longer chains.

3.6. Surface analysis of the polymeric films

SEM images were acquired to examine the morphological characteristics of the **PEDOT-TPPF$_{16}$** films. Fig. 6a and b displays images of the bare ITO electrode and the **PEDOT-TPPF$_{16}$** film, respectively. The porphyrin film uniformly covers the entire ITO surface, presenting a nearly smooth surface formed by the agglomeration of fused spherical particles measuring about 10–20 nm (as also observed in AFM images, Fig. 6c and d) that follows the roughness pattern of ITO. The small spherical particles interconnect to form a network, creating a three-dimensional structure with void spaces. These void spaces within the film can create extensive contact areas between the liquid electrolyte and the film surface, establishing pathways for effective ion diffusion and migration.

The surface morphologies of the resulting polymer films were further analyzed using AFM. Fig. 6c and d depict typical acoustic AC mode AFM height images of the electrodeposited film on ITO. Consistent with previous reports on electrochemically generated porphyrin films from tetradentate monomers, globular-like microstructures are evident in the analyzed films.[55] This observed microstructure appears to result from the nucleation and subsequent growth processes, leading to a homogeneous decoration of the ITO surface. In agreement with this observation, the calculated root mean square roughness (Sq) of **PEDOT-TPPF$_{16}$** film is a little higher (1.9 ± 0.4 nm) than that of bare ITO (1.2 ± 0.2 nm). Fig. 6d illustrates that the polymer surface is highly homogeneous, completely covering the electrode.

3.7. Galvanostatic charge–discharge tests of the film

Owing to the film's reversible oxidation and reduction processes, with high cyclic stability, it can be anticipated that

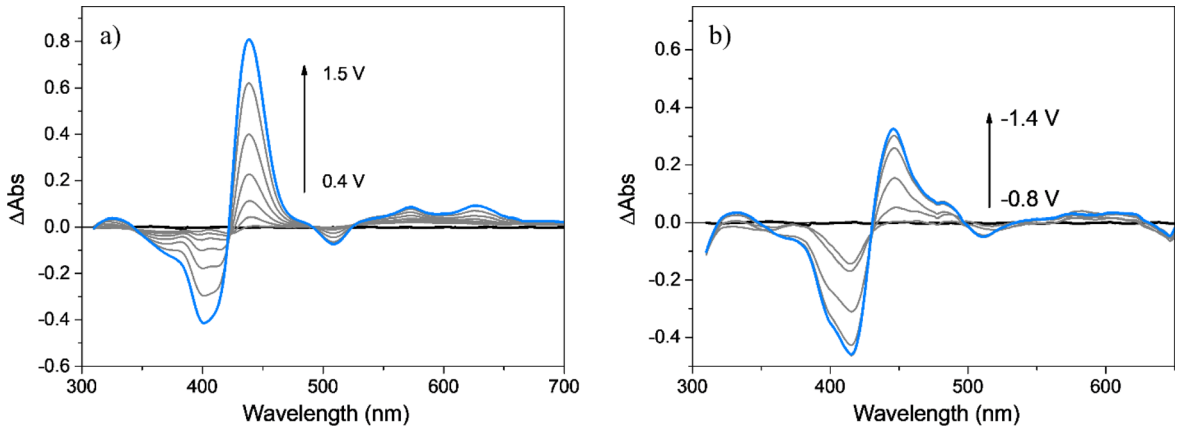

Fig. 5 Difference absorption spectra, ΔAbs, of: **PEDOT-TPPF$_{16}$** film deposited over ITO electrode obtained at different applied potentials: (a) 0.4 (black line), 0.9 to 1.4 (gray lines) and 1.5 V (cyan line); (b) −0.8 (black line), −0.9 to −1.3 (gray lines) and −1.4 V (cyan line). All measurements were conducted in ACN (0.10 M TBAP) at 20 mV s^{-1}.

the polymer pseudo-capacitive behaviour could render it suitable as an active component in the development of supercapacitor devices.[87] To examine the effectiveness of the polymer as an active material for supercapacitors, we conducted GCD experiments at varied current densities in a three-electrode configuration (ACN 0.10 M, TBAP). The oxidation onset and

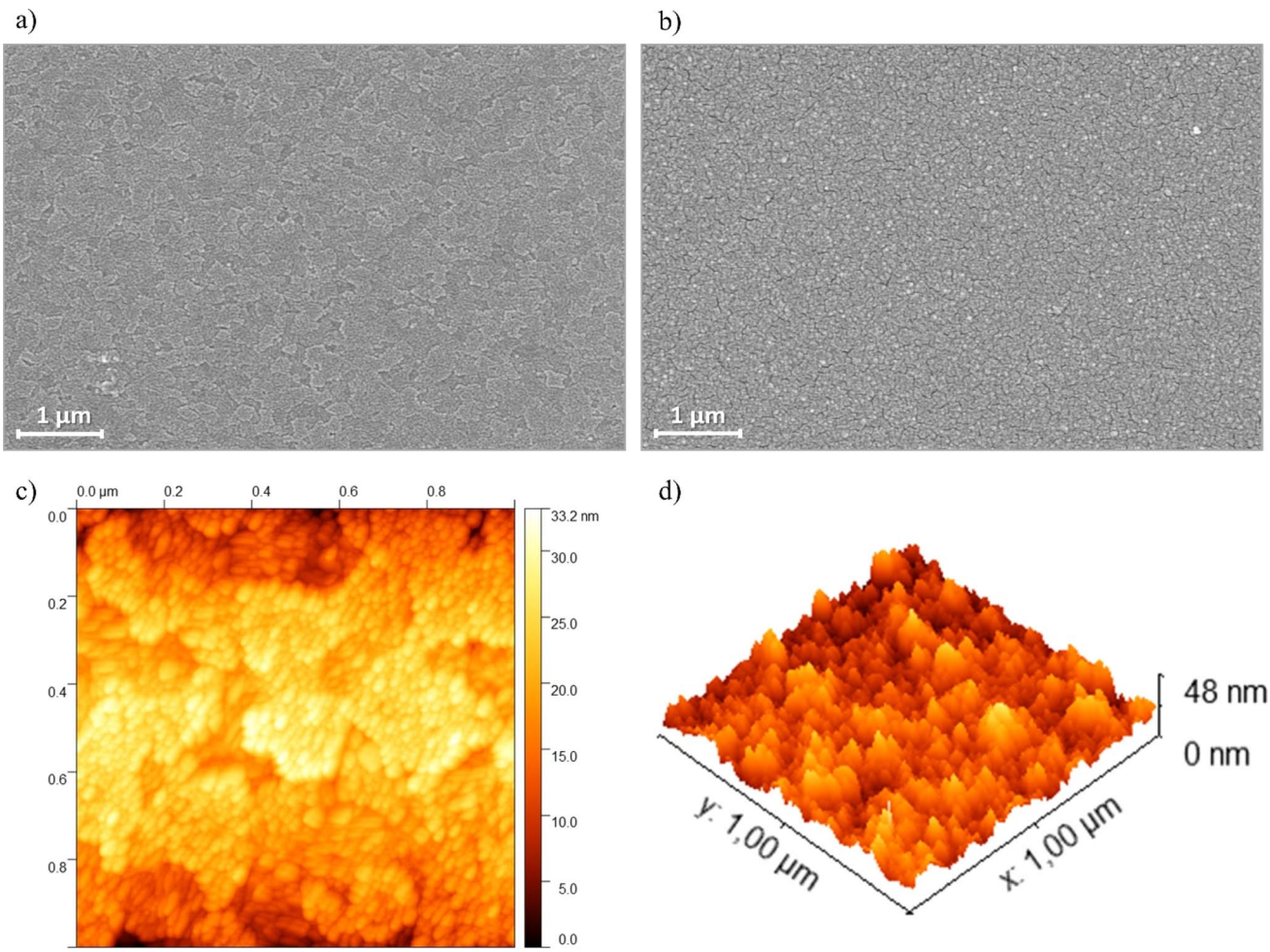

Fig. 6 SEM images of (a) bare ITO and (b) **PEDOT-TPPF$_{16}$** film. Scale bars are 1 µm. (c) AFM images of ITO electrode surface (scan size 1 × 1 µm) registered after electrodeposition of porphyrin film. (d) Three-dimensional representation of the electrode surfaces measured by AFM. Films were grown cycling in the same conditions of the exhibited in Fig. 3.

cutoff potentials were within the range of 0.0–1.0 V (Fig. 7a), while the reduction onset and cutoff potentials were within the range of 0.0 to −1.0 V (Fig. 7b), after the initial reduction peak, as observed in the CV experiments. During the oxidation processes, the voltage undergoes a rapid vertical ascent within the 0 to 0.4 V range. The energy stored in this interval, attributed to the electronic double-layer capacitance, is considered negligible.[88,89] On the other hand, within the potential range of 0.4–1.0 V, the responses display a quasi-triangular charge–discharge behavior at various current densities, arising from the pseudocapacitance associated with the reversible redox processes observed in the polymeric material.[55,58,90] The charge and discharge curves exhibit nearly symmetrical patterns, indicative of a rapid and reversible electron exchange.[91] Furthermore, with increments in the current density, both charge and discharge times experience notable reductions. However, it is noteworthy that even at elevated current regimes of up to 50 A g^{-1}, the film exhibits a specific capacitance retention of approximately 75%, as illustrated in Fig. 7c. Likewise, in the reduction process, charge–discharge curves exhibited similar behavior (Fig. 7b and c), with quasi-triangular performances, but displaying fast potential changes at applied potential close to the redox peak, in agreement with the observed in CV experiments. **PEDOT-TPPF$_{16}$** exhibits maximum specific capacitances of 140 F g^{-1} and 330 F g^{-1} (calculated from the discharge curves) for the oxidation and reduction processes, respectively, at a current density of 10 A g^{-1}. These values are inferior to those reported for supercapacitors based on hydrogen-bonded metal porphyrin frameworks,[92] but similar to the values reported for electrogenerated porphyrin polymers.[26,55,87,92]

The observed asymmetry in GCD during the n-doping process (Fig. 7b) could be originated in the leakage process resulting from oxygen reduction reaction. n-doped polymers are less common due to their low stability in the doped state and their tendency to be de-doped by transferring electrons to ambient oxygen.[93]

Additionally, to further explore into the polymeric material electronic behavior analysis, we conducted EIS experiments in a three-electrode configuration (ACN 0.10 M, TBAP). Fig. 7d exhibits the Nyquist plot that we obtained for a thin film electrode generated in the same condition as the one depicted in Fig. 2a. The gathered data was fitted through the Randles equivalent circuit, illustrated in the inset of Fig. 7d, using the EIS Spectrum Analyzer software. The equivalent circuit includes

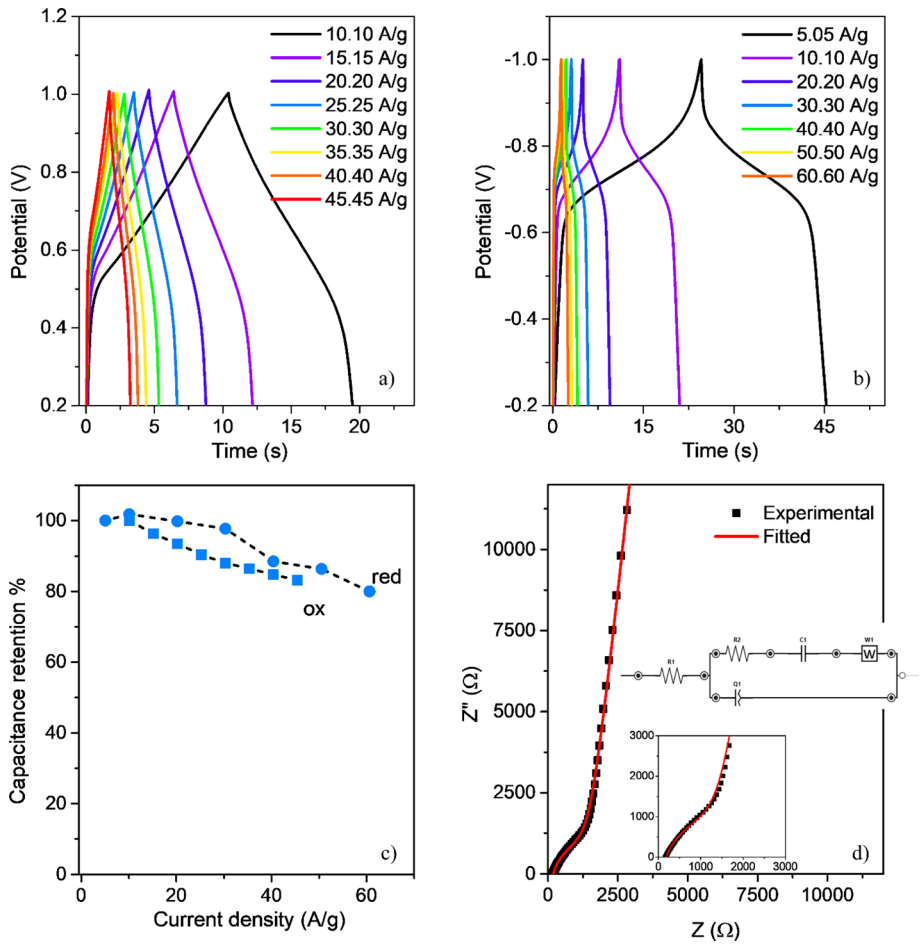

Fig. 7 (a) Oxidation and (b) reduction galvanostatic charge/discharge cycles of PEDOT-TPPF$_{16}$ at different current densities. (c) Capacitance retention % of PEDOT-TPPF$_{16}$ (oxidation in blue squares and reduction in blue circles) (d) Nyquist plot of PEDOT-TPPF$_{16}$ at 1.0 V. PEDOT-TPPF$_{16}$ film was deposited on an GC electrode. All measurements were conducted in ACN containing 0.10 M TBAP.

an ohmic resistance (R_{ES}), an interfacial charge transfer resistance (R_{CT}), and two constant phase elements: C_{DL}, which represents an electric double-layer capacitance, and C_{PS}, which represents the pseudocapacitance of the electrode. The diffusion-controlled process into the electrode was simulated with a Warburg element (Z_w). The plot shows two regions. At high frequency, an equivalent series resistance (R_{ES}) is observed as a semicircle intercepting the real axis at 160 Ω. This represents the ionic and electronic resistance of the electrolyte and electrode, as well as the contacts. At low frequency, the Nyquist plot second region shows the electrode capacitive behavior through a nearly vertical line. The fitted data provided a gravimetric capacitance of 120 F g^{-1}, similar to the value obtained from charge–discharge experiments.

4. Conclusions

This work presents the synthesis of a new fluorinated porphyrin, **EDOT-TPPF$_{16}$**, and the subsequent electrochemical synthesis of polymeric films, **PEDOT-TPPF$_{16}$**. The monomer design combines the robust perfluorinated porphyrin, known for its exceptional photo and chemical stability, with the versatile and widely used electropolymerizable EDOT group. The electrochemical polymerization of **EDOT-TPPF$_{16}$** generated electroactive polymeric films that showed promising pseudocapacitive behavior in energy storage devices. Various techniques were used to characterize the films. These presented gravimetric capacitances of 140 F g^{-1} and 330 F g^{-1} for the cathodic and anodic processes, respectively, at a current density of 10 A g^{-1}. To the best of our knowledge, this is the first time that a perfluorinated porphyrin substituted with EDOT is electropolymerized, representing an important advancement in the field of electroactive polymeric materials.

Author contributions

Conceptualization, E. B. P., E. J. G. L., C. A. S., J. C. L., L. P. M., R. E. D., Y. B. P., E. N. D., L. A. O., M. A. G. and D. A. H.; methodology, E. B. P., E. J. G. L., C. A. S., J. C. L., L. P. M., R. E. D., Y. B. P., E. N. D., L. A. O., M. A. G. and D. A. H.; validation, E. B. P., E. J. G. L., C. A. S., J. C. L., L. P. M., R. E. D., Y. B. P.; investigation, E. B. P., E. J. G. L., C. A. S., J. C. L., L. P. M., R. E. D., Y. B. P.; data curation, E. B. P., E. J. G. L., C. A. S., J. C. L., L. P. M., R. E. D., Y. B. P., E. N. D., L. A. O., M. A. G. and D. A. H.; writing—original draft preparation, C. A. S., L. P. M., L. A. O., M. A. G. and D. A. H.; writing—review and editing, C. A. S., L. P. M., R. E. D., S. B. A., L. A. O., M. A. G. and D. A. H.; visualization, E. B. P., E. J. G. L., C. A. S., J. C. L., L. P. M., R. E. D., Y. B. P., E. N. D., L. A. O., M. A. G. and D. A. H.; supervision, C. A. S., L. A. O., M. A. G., and D. A. H.; project administration, C. A. S., L. A. O., M. A. G., and D. A. H.; funding acquisition, C. A. S., L. A. O., M. A. G., and D. A. H. All authors have read and agreed to the published version of the manuscript. Details of the experimental part: E. B. P., J. C. L., and C. A. S. conducted the electrochemistry and impedance measurements, and charge–discharge experiments. E. J. G. L., R. E. D., Y. B. P. and D. A. H. were responsible for the synthesis of the compounds and structure elucidation. L. P. M. performed the SEM and AFM studies. S. B. A. performed XDR and ATR-FTIR experiments.

Conflicts of interest

There are no conflicts to declare.

Acknowledgements

Authors are grateful to Secretaría de Ciencia y Técnica, Universidad Nacional de Río Cuarto (Secyt-UNRC), Consejo Nacional de Investigaciones Científicas y Técnicas (CONICET, PIBAA 2022–2023 28720210101120CO, PIBAA 2022–2023 28720210101058CO, PIP 2021–23 PIP 11220200101208CO) and Agencia Nacional de Promoción Científica y Tecnológica (ANPCYT, PICT 02391/19) of Argentina for financial support. C. A. S., L. P. M., S. B. A., E. N. D., L. A. O., M. A. G., and D. A. H. are scientific members of CONICET. E. B. P., E. J. G. L., J. C. L., Y. B. P. and R. E. D. thank CONICET for doctoral fellowship. The authors greatly acknowledge the technical and imaging assistance of staff from the Laboratorio de Nanoscopía y Nanofotónica (LANN) – CONICET – Universidad Nacional de Córdoba (UNC), Córdoba, Argentina.

References

1 J. Min Park, J. H. Lee and W.-D. Jang, *Coord. Chem. Rev.*, 2020, **407**, 213157.
2 R. Costa e Silva, L. Oliveira da Silva, A. de Andrade Bartolomeu, T. J. Brocksom and K. T. de Oliveira, *Beilstein J. Org. Chem.*, 2020, **16**, 917–955.
3 M. M. Al Mogren, N. M. Ahmed and A. A. Hasanein, *J. Saudi Chem. Soc.*, 2020, **24**, 303–320.
4 Y. Matsuo, K. Ogumi, I. Jeon, H. Wang and T. Nakagawa, *RSC Adv.*, 2020, **10**, 32678–32689.
5 Z.-L. Qi, Y.-H. Cheng, Z. Xu and M.-L. Chen, *Int. J. Mol. Sci.*, 2020, **21**, 5839.
6 C. C. Negut, R.-I. Stefan - van Staden and J. F. van Staden, *ECS J. Solid State Sci. Technol.*, 2020, **9**, 051005.
7 J. Chen, Y. Zhu and S. Kaskel, *Angew. Chem., Int. Ed.*, 2021, **60**, 5010–5035.
8 N. Rabiee, M. T. Yaraki, S. M. Garakani, S. M. Garakani, S. Ahmadi, A. Lajevardi, M. Bagherzadeh, M. Rabiee, L. Tayebi, M. Tahriri and M. R. Hamblin, *Biomater*, 2020, **232**, 119707.
9 J. Tian, B. Huang, M. H. Nawaz and W. Zhang, *Coord. Chem. Rev.*, 2020, **420**, 213410.
10 A. Akbar, S. Khan, T. Chatterjee and M. Ghosh, *J. Photochem. Photobiol., B*, 2023, **248**, 112796.
11 C. Comuzzi, M. Marino, D. Poletti, M. Boaro and P. Strazzolini, *J. Photochem. Photobiol., A*, 2022, **430**, 113967.
12 D. Das and S. Kurungot, *Energy Technol.*, 2020, **8**, 2000061.
13 M. Xie, J. Liu, L. Dai, H. Peng and Y. Xie, *RSC Adv.*, 2023, **13**, 24699–24730.
14 W. Chen, P. Chen, G. Zhang, G. Xing, Y. Feng, Y.-W. Yang and L. Chen, *Chem. Soc. Rev.*, 2021, **50**, 11684–11714.
15 Z. Li and Y.-W. Yang, *Polym. Chem.*, 2021, **12**, 4613–4620.

16 W. Ji, T.-X. Wang, X. Ding, S. Lei and B.-H. Han, *Coord. Chem. Rev.*, 2021, **439**, 213875.
17 Z. Li and Y.-W. Yang, *Adv. Mater.*, 2022, **34**, 2107401.
18 X. Li, C. Tang, L. Zhang, M. Song, Y. Zhang and S. Wang, *Biomimetics*, 2023, **8**, 171.
19 L. Shu, J. Yu, Y. Cui, Y. Ma, Y. Li, B. Gao and H.-g. Wang, *Int. J. Hydrogen Energy*, 2022, **47**, 10902–10910.
20 Y. Zhang, L. Cheng, L. Zhang, D. Yang, C. Du, L. Wan, J. Chen and M. Xie, *J. Energy Storage*, 2021, **34**, 102018.
21 Y. Wang, X. Cui, P. Zhang, Y. Wang and W. Lu, *Environ. Technol. Innovation*, 2023, **29**, 102972.
22 Q. Liu, Q. Sun, J. Shen, H. Li, Y. Zhang, W. Chen, S. Yu, X. Li and Y. Chen, *Coord. Chem. Rev.*, 2023, **482**, 215078.
23 W.-C. Wang, Y.-W. Lin, S.-H. Peng, C.-T. Chuang, C.-C. Chang and C.-S. Hsu, *Org. Electron.*, 2020, **86**, 105899.
24 Z. Liu, Z. Huang, Y. Chen, T. Xu, H. Yu, X. Guo, L. Yan, M. Zhang, W.-Y. Wong and X. Wang, *Macromol. Chem. Phys.*, 2020, **221**, 1900446.
25 J. Tian and W. Zhang, *Prog. Polym. Sci.*, 2019, **95**, 65–117.
26 J. E. Durantini, R. Rubio, C. Solis, L. Macor, G. M. Morales, M. I. Mangione, D. A. Heredia, E. N. Durantini, L. Otero and M. Gervaldo, *Sustainable Energy Fuels*, 2020, **4**, 6125–6140.
27 Z. Chen, J. Wang, S. Zhang, Y. Zhang, J. Zhang, R. Li and T. Peng, *ACS Appl. Energy Mater.*, 2019, **2**, 5665–5676.
28 Y. Zhang, L. Cheng, L. Zhang, D. Yang, C. Du, L. Wan, J. Chen and M. Xie, *J. Energy Storage*, 2021, **34**, 102018.
29 R. Guilard, K. M. Kadish, K. M. Smith and R. Guilard, *The Porphyrin Handbook*, Academic Press, New York, 2003.
30 R. Luo, M. Chen, F. Zhou, J. Zhan, Q. Deng, Y. Yu, Y. Zhang, W. Xu and Y. Fang, *J. Mater. Chem. A*, 2021, **9**, 25731–25749.
31 M. Gervaldo, M. Funes, J. Durantini, L. Fernandez, F. Fungo and L. Otero, *Electrochim. Acta*, 2010, **55**, 1948–1957.
32 J. Durantini, L. Otero, M. Funes, E. N. Durantini, F. Fungo and M. Gervaldo, *Electrochim. Acta*, 2011, **56**, 4126–4134.
33 H. Ma, Y. Chen, X. Li and B. Li, *Adv. Funct. Mater.*, 2021, **31**, 2101861.
34 B. Stöckle, D. Y. W. Ng, C. Meier, T. Paust, F. Bischoff, T. Diemant, R. J. Behm, K.-E. Gottschalk, U. Ziener and T. Weil, *Macromol. Symp.*, 2014, **346**, 73–81.
35 D. A. Heredia, E. J. Gonzalez Lopez, E. N. Durantini, J. Durantini, T. Dittrich, J. Rappich, L. Macor, C. Solis, G. M. Morales, M. Gervaldo and L. Otero, *Electrochim. Acta*, 2019, **311**, 178–191.
36 D. Heredia, L. Fernandez, L. Otero, M. Ichikawa, C.-Y. Lin, Y.-L. Liao, S.-A. Wang, K.-T. Wong and F. Fungo, *J. Phys. Chem. C*, 2011, **115**, 21907–21914.
37 T. Patois, B. Lakard, S. Monney, X. Roizard and P. Fievet, *Synth. Met.*, 2011, **161**, 2498–2505.
38 K. Cysewska, J. Karczewski and P. Jasiński, *Electrochim. Acta*, 2015, **176**, 156–161.
39 R. K. Gupta, *Organic Electrodes: Fundamental to Advanced Emerging Applications*, Springer Nature, 2022.
40 M. A. Soldatov, V. V. Butova, D. Pashkov, M. A. Butakova, P. V. Medvedev, A. V. Chernov and A. V. Soldatov, *Nanomaterials*, 2021, **11**, 619.
41 X. F. Lu, Y. Fang, D. Luan and X. W. D. Lou, *Nano Lett.*, 2021, **21**, 1555–1565.
42 S. H. Mir, L. A. Nagahara, T. Thundat, P. Mokarian-Tabari, H. Furukawa and A. Khosla, *J. Electrochem. Soc.*, 2018, **165**, B3137.
43 X. Zhang, Z. Xiao, X. Liu, P. Mei and Y. Yang, *Renewable Sustainable Energy Rev.*, 2021, **147**, 111247.
44 E. Reynoso, A. M. Durantini, C. A. Solis, L. P. Macor, L. A. Otero, M. A. Gervaldo, E. N. Durantini and D. A. Heredia, *RSC Adv.*, 2021, **11**, 23519–23532.
45 K. Sun, S. Zhang, P. Li, Y. Xia, X. Zhang, D. Du, F. H. Isikgor and J. Ouyang, *J. Mater. Sci.: Mater. Electron.*, 2015, **26**, 4438–4462.
46 S. Nie, Z. Li, Y. Yao and Y. Jin, *Front. Chem.*, 2021, **9**, 803509.
47 I. V. Shershnev, A. S. Kopylov, A. V. Cherkasova and A. B. Solovieva, *Russ. J. Phys. Chem. B*, 2022, **16**, 1277–1284.
48 A. S. Kopylov, N. A. Aksenova, M. A. Savko, I. V. Shershnev, T. S. Zarkhina, A. V. Krivandin, O. V. Shatalova, A. V. Cherkasova, P. S. Timashev and A. B. Solovieva, *Russ. J. Phys. Chem.*, 2022, **96**, 444–449.
49 D. Tao, L. Feng, Y. Chao, C. Liang, X. Song, H. Wang, K. Yang and Z. Liu, *Adv. Funct. Mater.*, 2018, **28**, 1804901.
50 Z. Yang, D. Tao, W. Zhong, Z. Liu, L. Feng and M. Chen, *Biomaterials*, 2022, **280**, 121250.
51 N. K. Zaitsev, P. V. Melnikov, V. A. Alferov, A. V. Kopytin and K. E. German, *Procedia Eng.*, 2016, **168**, 309–312.
52 M. Manathanath, M. Xie, C. Arunkumar, Z. Wang, J. Zhao and S. Sujatha, *Dyes Pigm.*, 2019, **165**, 117–127.
53 Q. Cao, Q. Yin, Q. Chen, Z.-B. Dong and B.-H. Han, *Chem.–Eur. J.*, 2017, **23**, 9831–9837.
54 C. Solis, E. Baigorria, M. E. Milanesio, G. Morales, E. N. Durantini, L. Otero and M. Gervaldo, *Electrochim. Acta*, 2016, **213**, 594–605.
55 R. Rubio, M. B. Suarez, M. E. Pérez, D. A. Heredia, G. M. Morales, E. N. Durantini, L. Otero, M. Gervaldo and J. E. Durantini, *Electrochim. Acta*, 2023, **458**, 142552.
56 H. Zhang, Y. Zhang, C. Gu and Y. Ma, *Adv. Energy Mater.*, 2015, **5**, 1402175.
57 E. J. Gonzalez Lopez, M. Renfige Rodriguez, S. C. Santamarina, L. Macor, L. A. Otero, M. A. Gervaldo, A. M. Durantini, E. N. Durantini, J. E. Durantini and D. A. Heredia, *ACS Appl. Polym. Mater.*, 2023, **5**, 943–956.
58 S. Zhang and N. Pan, *Adv. Energy Mater.*, 2015, **5**, 1401401.
59 C. J. Raj, M. Rajesh, R. Manikandan, S. Park, J. H. Park, K. H. Yu and B. C. Kim, *Ionics*, 2018, **24**, 2335–2342.
60 C. J. Raj, B. C. Kim, W.-J. Cho, W.-g. Lee, S.-D. Jung, Y. H. Kim, S. Y. Park and K. H. Yu, *ACS Appl. Mater. Interfaces*, 2015, **7**, 13405–13414.
61 D. A. Heredia, S. R. Martínez, A. M. Durantini, M. E. Pérez, M. I. Mangione, J. E. Durantini, M. A. Gervaldo, L. A. Otero and E. N. Durantini, *ACS Appl. Mater. Interfaces*, 2019, **11**, 27574–27587.
62 J. I. T. Costa, A. C. Tomé, M. G. P. M. S. Neves, J. A. S. Cavaleiro and J. Porphyr, *Phthalocyanines*, 2011, **15**, 1116–1133.
63 N. V. S. D. K. Bhupathiraju, W. Rizvi, J. D. Batteas and C. M. Drain, *Org. Biomol. Chem.*, 2016, **14**, 389–408.

64 M. C. Malacarne, S. Banfi, A. S. Alberton, E. Caruso and J. Porphyr, *Phthalocyanines*, 2019, **23**, 1047–1056.
65 D. A. Heredia, J. E. Durantini, D. D. Ferreyra, E. Reynoso, E. J. Gonzalez Lopez, A. M. Durantini, M. E. Milanesio and E. N. Durantini, *J. Photochem. Photobiol., B*, 2021, **225**, 112321.
66 E. J. Gonzalez Lopez, S. R. Martínez, V. Aiassa, S. C. Santamarina, R. E. Domínguez, E. N. Durantini and D. A. Heredia, *Pharmaceutics*, 2023, **15**, 392.
67 R. Lyubimenko, D. Busko, B. S. Richards, A. I. Schäfer and A. Turshatov, *ACS Appl. Mater. Interfaces*, 2019, **11**, 31763–31776.
68 W.-P. To, Y. Liu, T.-C. Lau and C.-M. Che, *Chem.–Eur. J.*, 2013, **19**, 5654–5664.
69 K. L. Kadish, K. M. Smith and R. Guilard, *The Porphyrin Handbook*, Academic Press, New York, 1999, vol. 8.
70 C. Brückner and N. Hewage, *Oxidation and Reduction of Porphyrins in Fundamentals of Porphyrin Chemistry*, ed. P. J. Brothers and M. O. Senge, 2022, pp. 303–347, DOI: **10.1002/9781119129301.ch6**.
71 Y. Cui, L. Zeng, Y. Fang, J. Zhu, C. H. Devillers, D. Lucas, N. Desbois, C. P. Gros and K. M. Kadish, *ChemElectroChem*, 2016, **3**, 228–241.
72 K. M. Kadish and M. M. Morrison, *J. Am. Chem. Soc.*, 1976, **98**, 3326–3328.
73 H. Randriamahazaka, V. Noël and C. Chevrot, *J. Electroanal. Chem.*, 1999, **472**, 103–111.
74 Q. Pei, G. Zuccarello, M. Ahlskog and O. Inganäs, *Polymer*, 1994, **35**, 1347–1351.
75 J. Roncali, P. Blanchard and P. Frere, *J. Mater. Chem.*, 2005, **15**, 1589–1610.
76 L. Groenendaal, G. Zotti, P.-H. Aubert, S. M. Waybright and J. R. Reynolds, *Adv. Mater.*, 2003, **15**, 855–879.
77 A. Blacha-Grzechnik, M. Krzywiecki, R. Motyka and M. Czichy, *J. Phys. Chem. C*, 2019, **123**, 25915–25924.
78 F. Zaar, S. Olsson, R. Emanuelsson, M. Strømme and M. Sjödin, *Electrochim. Acta*, 2022, **424**, 140616.
79 S. C. Santamarina, D. A. Heredia, A. M. Durantini and E. N. Durantini, *Polymers*, 2022, **14**, 4936.
80 S. V. Selvaganesh, J. Mathiyarasu, K. L. N. Phani and V. Yegnaraman, *Nanoscale Res. Lett.*, 2007, **2**, 546–549.
81 Q. Zhao, R. Jamal, L. Zhang, M. Wang and T. Abdiryim, *Nanoscale Res. Lett.*, 2014, **9**, 557.
82 B. Gupta, M. Mehta, A. Melvin, R. Kamalakannan, S. Dash, M. Kamruddin and A. K. Tyagi, *Mater. Chem. Phys.*, 2014, **147**, 867–877.
83 Q. Xie, Y. Xu, Z. Wang, C. Xu, P. Zou, Z. Lin, C. Xu, C. Yang, F. Kang and C.-P. Wong, *PLoS One*, 2016, **11**, e0166529.
84 C. Paliteiro and A. Sobral, *Electrochim. Acta*, 2005, **50**, 2445–2451.
85 R. A. Krüger, A. S. Terpstra and T. C. Sutherland, *CJC University of Calgary 50th Anniversary Virtual Issue*, 2016, vol. 1, pp. 214–220.
86 Y. Fang, Y. G. Gorbunova, P. Chen, X. Jiang, M. Manowong, A. A. Sinelshchikova, Y. Y. Enakieva, A. G. Martynov, A. Y. Tsivadze, A. Bessmertnykh-Lemeune, C. Stern, R. Guilard and K. M. Kadish, *Inorg. Chem.*, 2015, **54**, 3501–3512.
87 M. A. Gervaldo, Y. M. R. Rodriguez, R. A. Rubio, L. P. Macor, C. A. Solis, J. E. Durantini and L. A. Otero, in *Organic Electrodes: Fundamental to Advanced Emerging Applications*, ed. R. K. Gupta, Springer International Publishing, Cham, 2022, pp. 379–397, DOI: **10.1007/978-3-030-98021-4_20**.
88 C. Lei, F. Markoulidis, Z. Ashitaka and C. Lekakou, *Electrochim. Acta*, 2013, **92**, 183–187.
89 S.-M. Chen, R. Ramachandran, V. Mani and R. Saraswathi, *Int. J. Electrochem. Sci.*, 2014, **9**, 4072–4085.
90 X. Wu, X. Feng, J. Yuan, X. Yang, H. Shu, C. Yang, Z. liu, J. Peng, E. Liu, S. Tan and P. Gao, *Energy Storage Mater.*, 2022, **46**, 252–258.
91 T.-H. Le, Y. Kim and H. Yoon, *Polymers*, 2017, **9**, 150.
92 W. Zhao, J. Peng, W. Wang, B. Jin, T. Chen, S. Liu, Q. Zhao and W. Huang, *Small*, 2019, **15**, 1901351.
93 S. Debnath, C. J. Boyle, D. Zhou, B. M. Wong, K. R. Kittilstved and D. Venkataraman, *RSC Adv.*, 2018, **8**, 14760–14764.